ON THE SYNERGISTIC EFFECT OF DOXORUBICIN AND MITOMYCIN C AGAINST BREAST CANCER CELLS

Adam J. Shuhendler[1], Peter J. O'Brien[1], Andrew M. Rauth[2] and Xiao Yu Wu[1]*

[1]*Leslie Dan Faculty of Pharmacy, University of Toronto, and* [2]*Ontario Cancer Institute, Princess Margaret Hospital, Toronto, Ontario, Canada*

SUMMARY

The combination of doxorubicin and mitomycin C has been shown previously to result in supra-additive tumor cell killing *in vitro* in both murine and human breast cancer cells and *in vivo* against murine breast cancer cells. Median effect analysis was used to determine the significance and degree of interaction. The origin of this synergy was sought by evaluating the contribution of membrane efflux pump modulation, formaldehyde production, reactive oxygen species, DNA cross-linking, and DNA double-strand breaks to this effect. The interaction of mitomycin C and doxorubicin *in vitro* was found to be a true synergy whose mechanism was efflux pump-independent. DNA cross-links were only found to increase additively with co-administration of the drugs; however, a supra-additive increase in DNA double-strand breaks was observed. The results suggest that poisoning of topoisomerase IIα by doxorubicin may interact with drug-induced DNA cross-links to enhance the formation of DNA double-strand breaks. This interaction, together with glutathione depletion and mitomycin C-derived formaldehyde, may be the underlying mecha-

* Author for correspondence:
Xiao Yu Wu
Graduate Department of Pharmaceutical Sciences
Leslie Dan Faculty of Pharmacy
University of Toronto
144 College Street
Ontario, Canada, M5S 3M2
e-mail: sxy.wu@utoronto.ca

nism(s) of the synergy observed between mitomycin C and doxorubicin.

KEY WORDS

breast cancer, combination chemotherapy, DNA double strand breaks, doxorubicin, mitomycin C, median effect analysis, synergy

INTRODUCTION

Drug combination therapy has been investigated extensively for over 40 years to overcome the high failure rate of single agent chemotherapy, thus improving this treatment modality and quality of life of patients /1/. Chemotherapeutic cocktails have been explored in the clinical setting, since: (1) combining two or more drugs may result in additive tumor cell death with subadditive off-target toxicity due to the lower dose of the individual agents involved; and (2) a tumor may be sensitive to at least one drug in the combination if the drugs work through different cytotoxic mechanisms /2/. Additionally, combining drugs may improve pharmacodynamics. By including two or more agents that have both exclusive toxic actions and the potential for a toxic interaction, synergistic efficacy of the drugs can result. This would further enhance on-target toxicity in the face of lowered individual doses of the drugs and decreased off-target toxicity.

Doxorubicin (DOX) and mitomycin C (MMC) are chemotherapeutic agents whose efficacy is limited by severe toxicity, e.g. the cardiotoxicity of DOX and the myelosuppression of MMC. Furthermore, they are susceptible to multidrug resistance (MDR) defenses of cancer cells /3,4/. The MDR phenotype translates to low intracellular concentrations of the drugs in the tumor and ineffective chemotherapy even if high therapeutic doses are administered. Many efforts have been made to circumvent MDR and the aforementioned problems of

---

Abbreviations: MMC = mitomycin C; DOX = doxorubicin; MEA = median effect analysis; TIIα = topoisomerase II α; DSB = double strand break; ROS = reactive oxygen species; ABT = 1-aminobenzotriazole; DIC = dicumarol; GSH = glutathione; NQO1 = NAD(P)H quinone oxidoreductase 1; CYP450 = cytochrome P450 reductase; N-AC = *N*-acetylcysteine; BH = 1-bromoheptane; MDR = multidrug resistance.

breast cancer chemotherapy, including the use of MMC and DOX combination. The cocktail of MMC and DOX has been tested clinically against breast cancer, however with conflicting results. While one group reported no increased efficacy of DOX and MMC when co-administered over DOX alone /5/, the second group reported that higher efficacy was observed /6/. These different results might be explained by the inclusion of patients who had undergone previous rounds of chemotherapy, and who displayed a decreased combined drug efficacy in the first study but not in the second study. Moreover, the combination dose and scheduling used for the trials may not have been optimum.

To gain insight into the effects of DOX-MMC combinations and to provide a rationale for the combination regimens, Cheung *et al.* /7,8/ conducted extensive investigation of various scheduling and dose combinations. The results obtained in human and murine breast cancer cell culture /7,8/, and in heterotopic murine breast tumor mouse models /8/ have indicated that the combination of MMC and DOX results in supra-additive antitumor efficacy. If in fact MMC and DOX act in synergy, defining the parameters important to this interaction could result in the enhancement of antitumor efficacy at lower doses than currently used in the clinic, providing the patient with a more tolerable, clinically useful chemotherapy regimen due to decreased off-target toxicity. Hence one of the objectives of this study was to determine the actual synergy of DOX and MMC.

Understanding the mechanism of DOX-MMC interaction is a required first step in the rational design of their combination into an effective anti-cancer regimen relevant to the clinical treatment of breast cancer. Two common toxic endpoints in the individual pathways of metabolism of MMC /9,10/ and DOX /11-13/ have been identified: (1) the generation of reactive oxygen species (ROS), and (2) the generation of drug-DNA cross-links. Co-administration of DOX with the formaldehyde releasing pro-drug, AN-9, showed enhanced genotoxicity due to the formation of a DOX-formaldehyde adduct, doxoform, which covalently binds DNA /14/. Based on this finding it is proposed that the methanol lost from MMC during its proximal metabolic steps may act as a source of formaldehyde for the formation of doxoform, enhancing the number of drug-DNA cross-links and increasing the toxicity of the combination therapy /15/. It is possible that these cross-links may prove cytotoxic due to their

interaction with DOX-topoisomerase IIα-DNA complexes, which are known to result in DNA double-strand breaks (DSBs) /16/.

In the present study, various experiments and analyses were conducted to determine whether the supra-additive antitumor efficacy observed previously is a true synergy of DOX-MMC and to test whether there are changes in DNA cross-link frequency and DSBs enabled by MMC metabolism, and whether these changes are responsible for the interaction observed with the combination therapy of DOX and MMC. Proof of this synergistic interaction may lead to the development of clinically useful chemotherapeutic cocktails of DOX and MMC.

MATERIALS AND METHOD

Materials

Dimedone, 1-aminobenzotriazole (ABT), dicumarol, formaldehyde, ammonium acetate, glacial acetic acid, iodoacetic acid, sodium bicarbonate, β-NADH, β-NADPH, nitrotetrazolium blue, 2,4-dinitrofluorobenzene, *N*-acetylcysteine, 1-bromoheptane, phenazine methosulfate, methylene blue, mitomycin C, and doxorubicin hydrochloride and other chemicals were purchased from Sigma-Aldrich Canada (Oakville, ON, Canada). Alkaline comet assay and TUNEL assay (TiterTACS®) materials were purchased from R&D Systems, Inc. (Minneapolis, MN, USA). The BioRad® Protein Quantitation Kit was purchased from Bio-Rad Laboratories Inc. (Mississauga, ON, Canada). Wild type EMT6 murine breast carcinoma cells were obtained from Dr. I. Tannock at the Ontario Cancer Institute (Toronto, ON, Canada). All cell-culture plastic ware was purchased from Sarstedt (Montreal, QUE, Canada). Cell culture medium, α-modified Minimal Essential Medium (α-MEM), was obtained from the Ontario Cancer Institute (Toronto, ON, Canada). Fetal bovine serum (FBS) and trypsin were respectively purchased from Cansera International Inc. (Etobicoke, ON, Canada), and VWR International (Mississauga, ON, Canada).

Cell maintenance

EMT6 cells were grown in α-MEM supplemented with 10% FBS (growth medium) at 37°C in a humidified incubator with 5% CO_2 as monolayers in plastic flasks (VWR International, Mississauga, ON, Canada). Cell doubling times were typically 24 hours. When cells reached confluence, they were trypsinized and subcultured at 50-fold dilution. Every three months, cultures were renewed by returning to frozen stock cells.

Preparation of subcellular fractions

The cell fractions were prepared by differential centrifugation, as previously described for cells taken from male Sprague-Dawley rats /17/. Cytosolic, mitochondrial, and microsomal cell fractions were aliquoted into microcentrifuge tubes, and stored at -70°C for future use. The protein content of the fractions was determined with the BioRad® Protein Quantitation Kit, as described by the manufacturer.

Measurement of formaldehyde

Formaldehyde was measured in subcellular factions using a solution containing dimedone (5,5-dimethyl-1,3-cyclohexadione), which results in the trapping of formaldehyde by dimedone and acetic acid to form a fluorescent product /18/. Rat liver subcellular fraction (100 µl of approximately 8 mg protein/ml) was added to 2.0 ml of 100 mM KH_2PO_4 buffer at pH 7.40. To this, MMC and NAD(P)H were added to final concentrations of 50 µM and 200 µM, respectively. After 5, 15, and 30 minutes, 2 ml of dimedone working solution was added, and the mixture was vortexed and immersed in boiling water for 10 minutes. Dimedone working solution consisted of 25 g of ammonium acetate, 0.40 ml glacial acetic acid, 0.3 g dimedone, and 100 ml distilled-deionized water (DDI water). After boiling, the fluorescence intensity at excitation and emission wavelengths of 395 nm and 460 nm, respectively, was measured. For assays using the inhibitors ABT or dicumarol, a final concentration of 1 mM ABT or 5 µM dicumarol was incubated with 20 µl subcellular fraction in reaction buffer for 30 minutes at room temperature prior to the addition of the other components of the assay.

Measurement of total reactive oxygen species

Nitrotetrazolium blue, a non-specific free radical acceptor resulting in the formation of the blue diformazan chromophore with the addition of four electrons /19/, was used to detect total ROS evolved from drug metabolism in rat liver subcellular fractions. To each well of a 96-well plate (VWR International, Mississauga, ON, Canada) containing 185 µl of 100 mM KH_2PO_4 buffer at pH 7.4, was added 150 µM nitrotetrazolium blue, 20 µl of subcellular fraction, and 10, 20, or 40 µM DOX or MMC. As a positive control, the subcellular fraction and drug were omitted, and replaced by 50 µM phenazine methosulphate. The reaction was initiated with the addition of 200 µM NAD(P)H. After incubation at room temperature for 30 minutes absorbance was measured at 560 nm. For assays using the inhibitors ABT or dicumarol, 1 mM ABT or 5 µM dicumarol was incubated with 20 µl subcellular fraction in reaction buffer for 30 minutes at room temperature prior to the addition of the other components of the assay.

Determination of intracellular glutathione

Intracellular GSH levels were determined in EMT6 cells as previously described /20/. Cells were treated for 2 hours prior to cell harvest with 2 mM *N*-acetylcysteine and 400 µM 1-bromoheptane to increase and decrease GSH, respectively.

Alkaline comet assay

The extent of DNA cross-linking following drug treatment was quantified using a modified alkaline comet assay as previously described /21/. For all experiments, EMT6 cells were plated at 1×10^5 cells/ml and incubated for 24 hours at 37°C in 5% CO_2 atmosphere. Following drug treatment, cells were harvested through trypsinization, and exposed to 3.1 Gy of ^{132}Co γ-irradiation over 4 minutes, and kept on ice within ten seconds of completion of irradiation to prevent DNA repair. Comets were prepared as per the protocol of the manufacturer. Slides were photographed under a Zeiss LSM510 deconvolusion fluorescence microscope (Carl Zeiss Canada Ltd., Toronto, ON, Canada) using AxioVision® software and a FITC filter. Once the images were captured, the metric of tail moment was scored using

CometScore® software (TriTek Corp., VA, USA), which employed the following equation for tail moment:

Tail moment = (tail intensity)(total comet length – head diameter)

TUNEL assay

DNA double-strand breaks were detected by the R&D Systems TiterTACS® colorimetric apoptosis detection kit. Prior to processing, EMT6 cells were plated at 75×10^4 cells/well in a conical bottom 96-well plate. The cells were incubated for 24 hours at 37°C in 5% CO_2 atmosphere, after which time they were exposed to MMC or DOX alone and in combination for 1 hour. Cells were then processed as recommended by the manufacturer without modification.

Drug accumulation assay

Drug uptake was studied in EMT6 cells in culture described previously /22/. Briefly, 1×10^6 cells were plated in the wells of 24-well microplates and incubated in growth medium for 24 hours. The cells were then incubated with 2 μM DOX with and without 4 μM MMC for different time periods, as indicated in results. Cells were immediately washed twice with ice-cold PBS and detached with trypsin, followed by pelleting and resuspension in 1 ml of a 1:1 mixture of ethanol:0.3 M HCl. Samples of each time point were placed in a 96-well microplate and the amount of doxorubicin was quantified with a spectrofluorimeter with excitation and emission wavelengths of 475 nm and 533 nm, respectively.

Drug efflux assay

Drug efflux was monitored from cultured cells *in situ*, adapting a UV spectrometry method described previously /23/. Briefly, 20×10^3 cells were plated onto 1×4 cm glass coverslips and incubated in supplemented PBS for 2 hours. Supplemented PBS contained all of the amino acids in α-MEM, 5.5 mM glucose, 4 mM L-glutamine, 20 mM HEPES, and 10% FBS at pH 7.4. After two hours, the coverslips were placed in 5 ml of supplemented PBS, and incubated for a further 24 hours. Half of the coverslips were then exposed to 1 μM DOX with and without 2 μM MMC for 2 hours, while the other half remained as

untreated controls. The cells were then washed twice with ice-cold PBS, and transferred to cuvettes containing 3 ml of supplemented PBS, pre-warmed to 37°C, such that each cuvette contained two coverslips, each at opposing walls of the cuvette. Drug efflux was monitored at 480 nm for 65 minutes at 37°C, after which time the difference in A480 nm between the drug-loaded and control cells was calculated.

Clonogenic assay

EMT6 cells were plated at 1×10^5 cells/ml and incubated for 24 hours at 37°C in 5% CO_2 atmosphere. After 1 hour incubation with DOX and MMC as single agents or in combination, cells were washed and detached by trypsinization. The cells were replated at 100 or 1,000 cells per dish. Cell cultures were then incubated for one week at 37°C in a humidified incubator with a mixture of 95% air and 5% CO_2, allowing viable cells sufficient time to grow into macroscopic colonies. The cells were fixed and stained with a 0.5% solution of methylene blue in 70% ethanol. The number of colonies formed was counted on a light table, from which plating efficiencies were calculated. The control plating efficiency for EMT6 cells was found to be 73 ± 4%. Normalized surviving fractions were determined by dividing the plating efficiency of the drug-treated cells by that of cells without exposure to the drug (i.e. the control) /24/. For inhibitor studies, cells were pre-incubated for 1 hour with 100 μM ABT or 100 μM dicumarol, or for 2 hours with 2 mM *N*-acetylcysteine or 400 μM 1-bromoheptane, prior to drug treatment.

Median effect analysis

Median effect analysis, a mathematical treatment of drug interactions derived from the mass-action law, was employed to analyze the results from the clonogenic assay /25,26/. As per the clonogenic assay method, cells were treated with five concentrations of MMC, five of DOX, and five of MMC and DOX in combination at a constant molar ratio of 2:1, and assayed for colony forming ability. The median effect plot of $\log[(f_a)^{-1}-1]^{-1}$ versus $\log[D]$ was generated, where f_a is the fraction of cells affected unable to form colonies, and D is the drug concentration. From this plot, both the slope *m*, a measure of the sigmoidicity of the dose-effect relationship, and D_m (x-intercept), the

median effect dose, were determined for each drug and for the combination of drugs. The combination index plot was generated as previously described /25/. The dose of agent 1, agent 2, and both agents together that affect x% of the plated colonies, D_{x1}, D_{x2}, $D_{x1,2}$, respectively, was calculated from Equation 1:

$$D_x = D_n\left[\frac{f_a}{1-f_a}\right]^{\frac{1}{m}} \qquad (Eq.\ 1)$$

Finally, the combination index (CI) was calculated for mutually non-exclusive drugs, using Equation 2 /25,26/:

$$CI = \frac{D_1}{D_{x1}} + \frac{D_2}{D_{x2}} + \frac{D_1 D_2}{D_{x1} D_{x2}} \qquad (Eq.\ 2)$$

CI is the ratio of the expected effect (D) to the observed effect of the drugs given in combination (D_x). The expected effect is calculated under the assumption of an additive effect. The observed combined efficacy ($D_{x1,2}$) is multiplied by the molar fraction of each drug in the combination, where P and Q are the fractional concentrations of MMC and DOX, respectively. The expected effect of each drug can be calculated from Equations 3a and 3b /25,26/:

$$D_1 = D_{x1,2}\left(\frac{P}{P+Q}\right) \qquad (Eq.\ 3a)$$

$$D_2 = D_{x1,2}\left(\frac{Q}{P+Q}\right) \qquad (Eq.\ 3b)$$

Statistical analyses

Data are presented as the means ± SD for results obtained from three independent trials. Statistical significance between two groups was tested with Student's t-test in MS Excel®. Significance between three or more groups was determined using one-way, two-way, or nested ANOVA, depending on the experiment, followed by a *post hoc* Tukey's Honestly Significant Difference test using Minitab v.12®. Tukey's test for non-additivity was performed with SPSS v.14®, testing the hypothesis that there is no multiplicative effect of the treatments in combination.

RESULTS

Median effect analysis

The response of EMT6 cells to treatment with MMC and DOX alone and in combination was quantified through measurements of cell clonogenic potential. MMC was less effective on a molar basis at preventing clonogenic expansion than was DOX (Fig. 1A). The efficacy of tumor cell killing was significantly enhanced when the chemotherapeutic agents were applied concurrently to the EMT6 monolayer.

The dose-response seen in Figure 1A was linearized into a median effect plot (Fig. 1B). As outlined by Chou and Talalay /25/, non-parallel curves in the median effect plot indicate that the two drugs act non-exclusively in the cell, demonstrating that the toxic endpoints of each drug are not the same, and the drugs do not compete for the same targets. This provides evidence that the increased effect of the co-application of MMC and DOX as seen from the dose-response curve depends on the combined action of the drugs, and not just their exclusive toxic mechanisms in the cancer cell. For this specific drug co-therapy, the combination index analysis shows that MMC and DOX interact synergistically in EMT6 cells (Fig. 1C).

The parameters of the drugs applied alone and in combination to the cells are defined in Table 1. The parameter *m* is a measure of the sigmoidicity of the dose-response curve. The correlation coefficient (R^2) determines whether the drugs obey the mass-action principle. Since the value of R^2 for each treatment group is greater than 0.90, the data used for the median effect analysis here obey the law of mass-action. The median-effect dose, or D_m, is the dose required of the specific drug treatment to kill 50% of the cells originally plated. As expected from the dose-effect curve in Figure 1A, MMC has a D_m approximately 5-fold that of DOX. Unexpectedly, the D_m of the combined drug treatment is greater than that of DOX alone (Table 1). Upon inspection of the median effect plot, the efficacy of the DOX and MMC co-application becomes less than that of DOX at concentrations of DOX below 1 μM, where the combination curve crosses the curve for DOX alone (Fig. 1B). However, at higher concentrations of DOX, and at levels of cell death beyond 4% (X in Fig. 1B), there is a significantly enhanced degree of tumor cell death with co-

administration over single drug use, which is corroborated by the combination index analysis at low fractional percent killing (Fig. 1C).

Drug accumulation and drug efflux

Efflux pump-mediated resistance to DOX and MMC is a well known occurrence in breast tumor cells such that modulation of this efflux action could account for the observed synergy /27/. The study of the effect of a drug combination on drug efflux necessitates the determination of the effect of that combination on drug accumulation, as lowered efflux may in fact be a result of impaired drug uptake. Co-incubation of cells with MMC and DOX resulted in a significant reduction of DOX accumulation beyond 120 minutes (Fig. 2A). However, MMC had no significant effect on the accumulation of DOX in EMT6 cells up to 120 minutes, the incubation time chosen for the drug efflux study. Therefore any change in drug efflux can be attributed to the drug efflux process, and not to differences in drug accumulation. Our results show that there is no significant difference in DOX efflux from EMT6 cells when the cells are incubated with DOX or concurrently with DOX and MMC for up to 60 minutes (Fig. 2B).

Reactive oxygen species

One of the biochemical parameters of toxicity that may contribute to the observed synergy is the production of ROS by both MMC /28-30/ and DOX /31/ following reductive metabolism. Both superoxide and hydroxyl radicals were detected using the radical electron trapping agent, nitrotetrazolium blue. Nitrotetrazolium blue itself was either metabolized by the NAD(P)H-dependent bioreductive enzymes present in the subcellular fractions, or was sensitive to the electron transfers that occur between the cofactors and the active site metals of the enzymes, resulting in a background level of formazan that was produced during the metabolic studies. Based on the level of this background, significant ROS were only detected when the levels of formazan formed gave absorbance readings above 0.243 at 560 nm. It was determined that any significant increase in ROS was only seen when DOX was incubated with NADPH in the cytosolic and microsomal fractions (data not shown). No significant ROS were detected from MMC, or from DOX in the mitochondria plus or minus

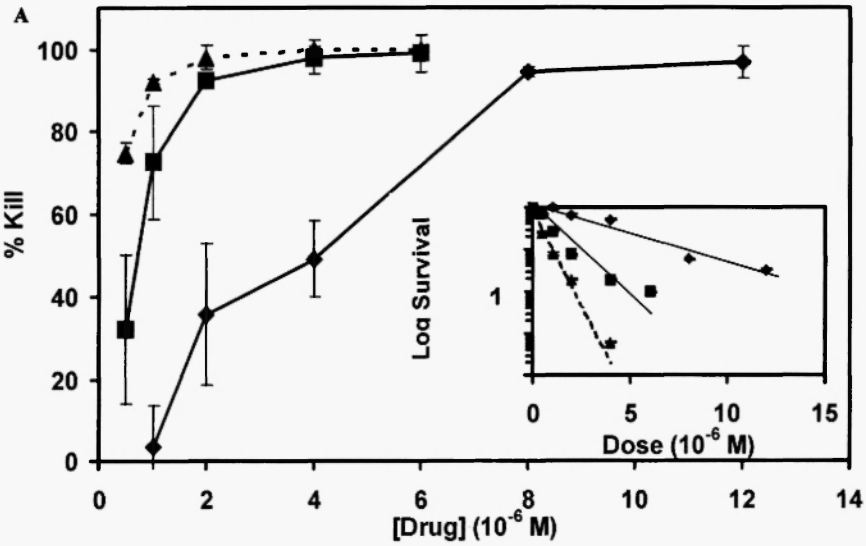

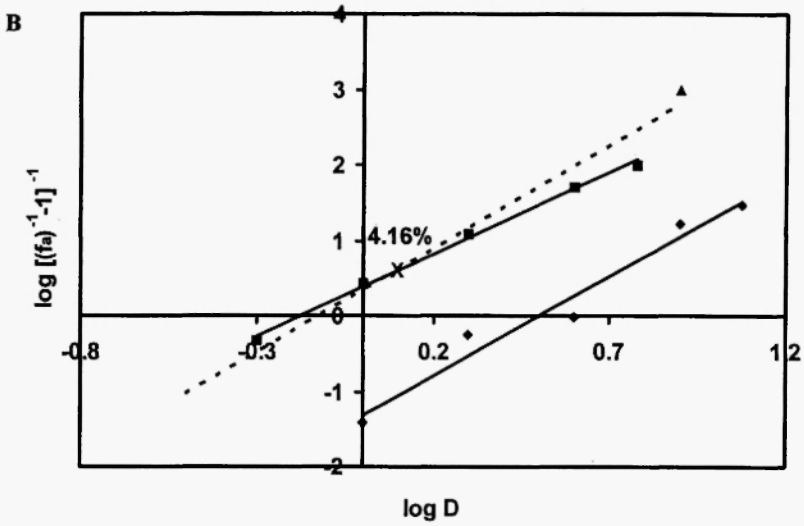

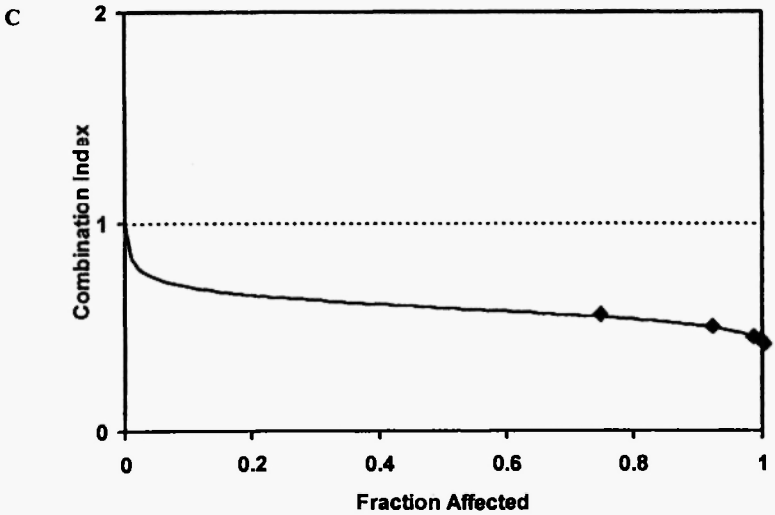

Fig. 1: Median effect analysis for the interaction of mitomycin C (MMC) and doxorubicin (DOX) in EMT6 cells. **A.** Dose-effect curve for the ability of EMT6 cells to expand clonogenically after treatment with MMC and DOX, alone and in combination. The cells were treated for 1 hour with MMC (◆), DOX (■), and MMC and DOX at a 2:1 molar ratio (- -▲- -). *Inset:* A plot of the cell survival vs dose (μM) of drug applied. Data points represent the mean ± standard deviation of three independent trials. **B.** Median effect plot for the interaction of MMC and DOX in EMT6 cells, following 1 hour drug exposure. **C.** Combination index (CI) analysis of the interaction of MMC and DOX in EMT6 cells following 1 hour of treatment. Values of combination index greater than 1 indicate antagonism, equal to 1 represent additivity, and less than 1 represent synergism. ◆ indicates the efficacy of the actual drug combinations employed on the generated CI curve.

TABLE 1

Summary table of the parameters of the action of mitomycin C (MMC) and doxorubicin (DOX) alone and in combination, as defined by the median effect analysis plot (Fig. 1B)

	MMC	DOX	MMC + DOX
D_m (μM)	3.17	0.67	0.75
m	2.64	2.17	2.73
R^2	0.965	0.997	0.962

D_m is the dose at which 50% of the cells are killed. m is a measure of the sigmoidicity of the curve. The correlation coefficient (R^2) must be greater than 0.90 for the observations to conform to the law of mass action.

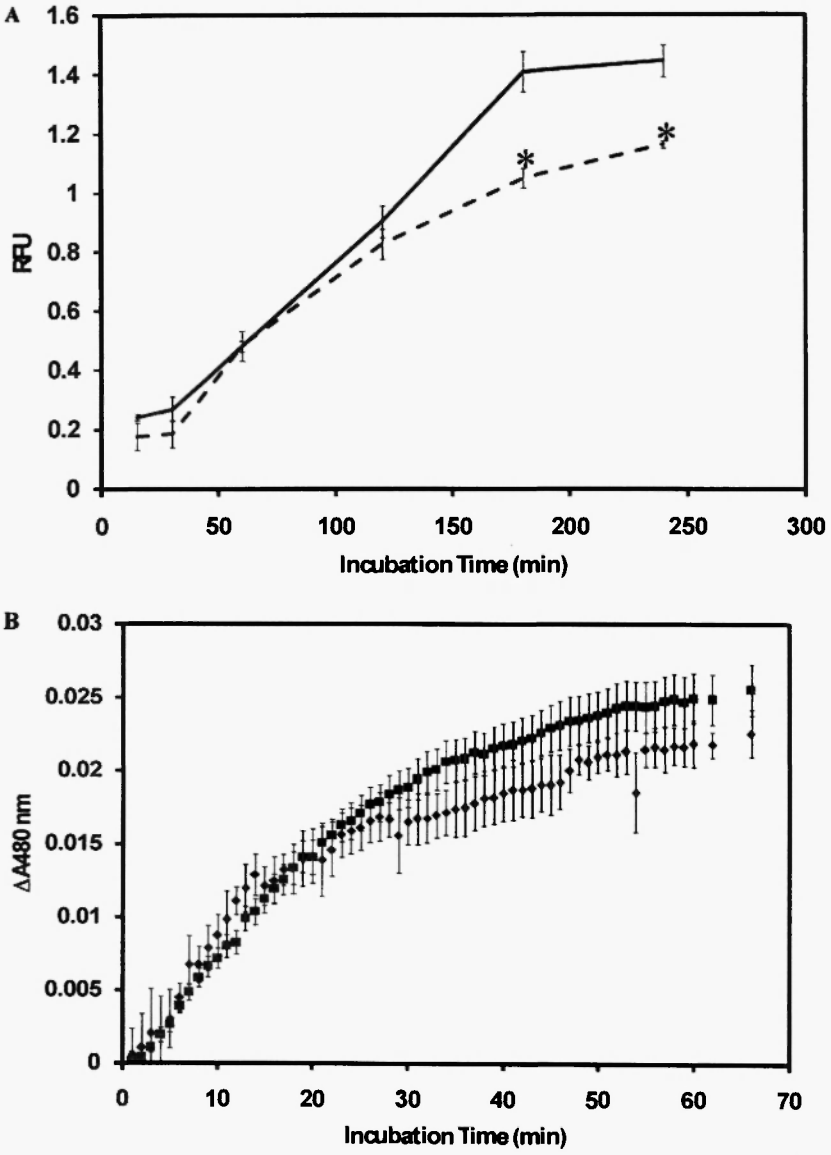

Fig. 2: The effect of doxorubicin (DOX) and mitomycin C (MMC) co-therapy on the accumulation and efflux of DOX from EMT6 cells. **A.** The accumulation of 2 μM DOX in EMT6 cells alone (solid line) or with 4 μM concurrent MMC (dashed line). **B.** The efflux of 1 μM DOX from EMT6 cells alone (■) or with 2 μM concurrent MMC (◆). Data represent the mean ± standard deviation of three independent trials. * Statistically significant decrease in the accumulation of DOX with and without MMC exposure ($p < 0.05$).

NADH (data not shown). As a result, the contribution of ROS to the synergy observed between DOX and MMC in the present study is at best questionable, if present.

Formaldehyde

The dimedone method for formaldehyde trapping was chosen based on the increased stability of the formed formaldehyde conjugate relative to those formed through the use of the Nash reagent, and due to the increased sensitivity afforded through fluorescence spectrophotometry /18,32/. The dimedone method resulted in a linear relationship between the concentration of formaldehyde and the relative fluorescence intensity (relative fluorescence unit [RFU] = 86.9 [formaldehyde], R^2 = 0.993), and was found to reliably detect formaldehyde as low as 0.05 μM (data not shown).

The evolution of formaldehyde from MMC was detected across all subcellular fractions (Fig. 3A,B). In the microsomal fraction the total concentration of formaldehyde produced was 2.4% and 1.8% of the total MMC concentration, with NADPH (Fig. 3A) and NADH (Fig. 3B), respectively. The cytosol and mitochondria resulted in 1.2% and 0.6% fractional formaldehyde evolution with NADPH, and 1.7% and 0.4% fractional evolution of formaldehyde with NADH, respectively. The low fractional evolution from MMC may be due to the high capacity of mammalian cells to rapidly detoxify formaldehyde with GSH-dependent aldehyde dehydrogenases /33/, due to its rapid formation of Schiff bases with protein amino groups /34/, or due to decreased aerobic metabolism of MMC /28,29/.

The generation of formaldehyde was time-dependent and the evidence indicated enzymatic involvement (Table 2). There was also a significant difference in the amount of formaldehyde evolved between the cell fractions, with the microsomal and cytosolic fractions being the major producers (Fig. 3A,B, Table 2). However, there was no significant difference in the evolution of formaldehyde between NADPH and NADH, indicating that the enzyme responsible is capable of using both cofactors with equal affinity. This finding provided evidence for the role of NAD(P)H quinone oxidoreductase 1 (NQO1) in the metabolism of MMC, as it is able to utilize both NADH and NADPH in 2-electron reductions /35/. In all three subcellular fractions, dicumarol reduced the level of formaldehyde produced to below 20% of the uninhibited activity level, providing support for the

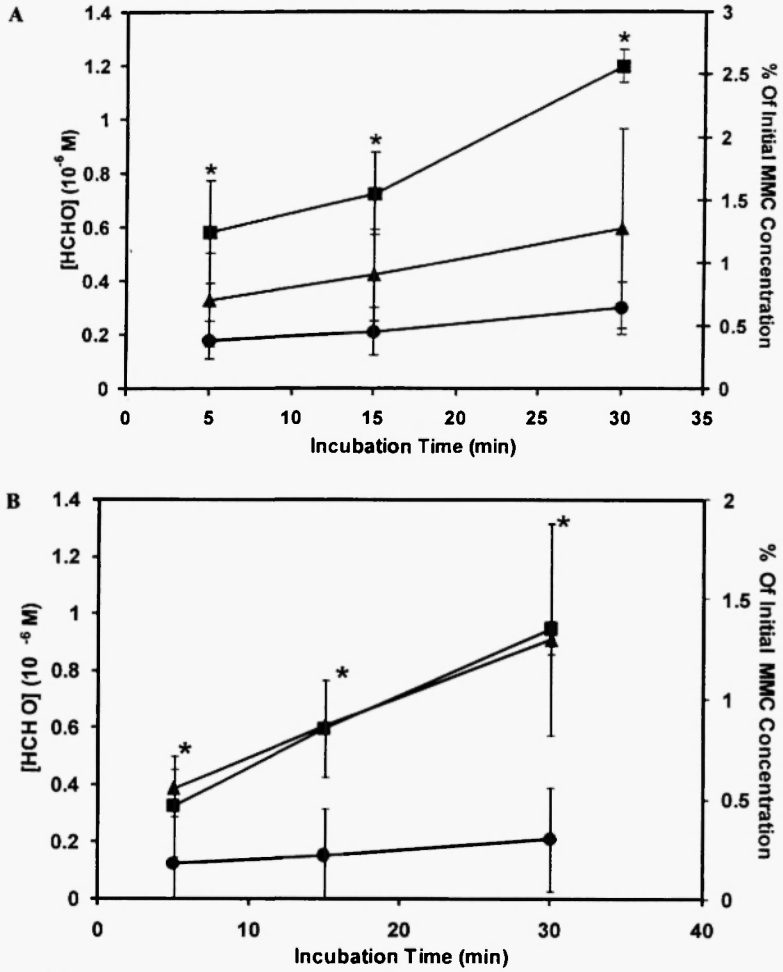

Fig. 3: Evolution of formaldehyde from the metabolism of 50 μM mitomycin C (MMC) in microsomes (■), cytosol (◆), and mitochondria (▲) with (**A**) NADPH and (**B**) NADH as the cofactor. The concentration of formaldehyde evolved was calculated from the fluorescence signal increase above the background level. **C.** The enzymology of the evolution of formaldehyde from the metabolism of MMC in microsomes, cytosol, and mitochondria. Dicumarol and NADH (grey) was used to inhibit NAD(P)H quinone oxidoreductase 1 (NQO1), and 1-aminobenzotriazole (ABT) and NADPH (black) was used to inhibit cytochrome P450 reductase. Data represent the mean ± standard deviation of three independent trials. * Statistically significant increase in formaldehyde evolution relative to other subcellular fractions at that time point ($p < 0.05$). ǂ Statistically significant inhibition relative to uninhibited control ($p < 0.05$).

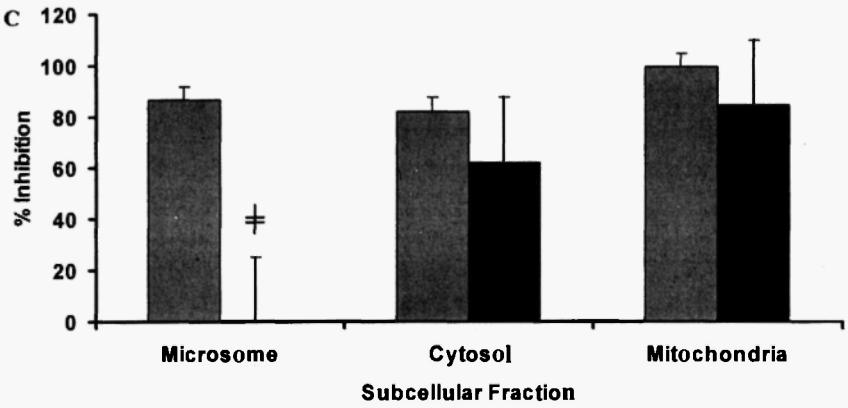

Fig. 3C

TABLE 2

Summary table for fixed factor, nested ANOVA of formaldehyde concentration

Source	df	SS	MS	F	p
Cell fraction	2	2.631	1.315	10.30	<0.05
Cofactor on cell fraction	3	0.379	0.126	0.86	>0.05
Incubation time on cofactor on cell fraction	12	1.758	0.147	5.51	<0.001
Error	36	0.957	0.027		
Total	53	5.727			

Within the cell fraction, cofactor, and incubation time factors, there were 3, 2, and 3 levels, respectively. df = degrees of freedom; SS = sum of squared errors; MS = mean of squared errors; F = F-ratio; p = probability value of F ratio.

involvement of NQO1 in formaldehyde production from MMC (Fig. 3C). The inhibition of cytochrome P450 reductase with ABT reduced formaldehyde production in cytosolic and mitochondrial fractions only (Fig. 3C). This suggests that in the microsomal fraction the sole metabolizer of MMC is the soluble NQO1 enzymes that exist within the endoplasmic reticulum.

Metabolic analysis in whole cells

By using the NQO1 specific inhibitor dicumarol and the cytochrome P450 reductase-specific inhibitor ABT, the importance of reductive activation of these drugs in the synergistic mechanism of interaction was investigated. Inhibition of CYP450 resulted in 20% increase in cell survival (Fig. 4A). Similarly, treatment with dicumarol resulted in 32% increase in cell survival. These results agree with the subcellular formaldehyde data, providing further evidence that formaldehyde is potentially an important player in the mechanism of drug synergy. Independent of formaldehyde, metabolic activation of the drugs, especially by NQO1, is important for the observed drug toxicity; however, the level of inhibition of bioreductive metabolism achieved here with ABT and DIC does not completely abrogate the toxicity of the drug combination. Important to the mechanism of interaction, then, is a toxic endpoint that is independent of drug activation.

Modulation of glutathione levels in whole cells

The toxicity of drug therapy was modulated through the alteration of intracellular levels of GSH. GSH levels were enhanced by 61% and depleted by 82% with 2 hours of incubation of EMT6 cells with *N*-acetylcysteine and 1-bromoheptane, respectively (Fig. 4B). The resting GSH level in EMT6 cells was found to be 27 ± 0.06 nM/10^6 cells. Previous measurements of resting intracellular GSH levels in Chinese Hamster ovary /36/, small-cell lung cancer (GLC4) /37/, and human colon cancer (HCT-116) /38/ cells have yielded values of 13-18 nM, 16 nM, and 14-21 nM, respectively. These values are of the same order of magnitude as the intracellular GSH concentration found in EMT6 cells here. Enhancement of intracellular GSH levels prior to drug treatment showed a marked enhancement of plating efficiency of cells treated with DOX and MMC relative to cells without treatment

with *N*-acetylcysteine (Fig. 4C). GSH depletion on its own was found to be toxic to EMT6 cells, decreasing plating efficiency below 60%. 1-Bromoheptane in conjunction with DOX and MMC significantly decreased the plating efficiency of EMT6 cells. By increasing the GSH levels in the cells treated with both MMC and DOX (Fig. 4C), the plating efficiency of EMT6 cells was increased to a significantly greater extent than it was by using enzyme inhibitors (Fig. 4A). This result suggests that, in the combined effect of these chemotherapeutic agents, the role of GSH and, perhaps more mechanistically important here, GSH-reactive species, such as formaldehyde, is an important one.

DNA cross-linking

Separately, both MMC /39,40/ and DOX /41/ have been shown to form interstrand DNA cross-links, among other monofunctional and bifunctional adducts, with the interstrand cross-links correlating well with cytotoxicity /42/. As hypothesized, it is expected that co-administration of the drugs would result in enhanced DNA cross-linking through an increased population of DNA alkylating agents, including the formation of the formaldehyde-conjugated, DNA-reactive form of DOX, doxoform.

In order to quantify the extent of DNA cross-linking following drug treatment the comet assay was used. The tail moment, a product of the intensity of the comet tail and the length of the tail, was calculated. The shorter the comet tail, the greater the size of the DNA fragments produced following ^{132}Co γ-irradiation due to cross-links between otherwise smaller fragments. Simultaneous treatment of EMT6 cells in culture with MMC and DOX resulted in a significant 10-15% decrease in tail moments relative to solo treatment of cells with either of these drugs (Fig. 5). When tested for additivity, the hypothesis of no multiplicative effect of the combination drug treatment on the percent tail moment decrease was unable to be rejected ($p = 0.131$), and the effect was shown to be additive. This suggests that, on its own, the summation of the bifunctional DNA adducts formed by both of these drugs may not account for the synergy observed between MMC and DOX in EMT6 cells.

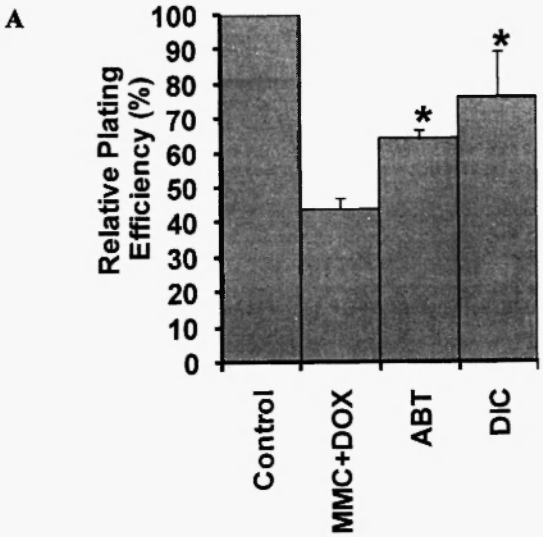

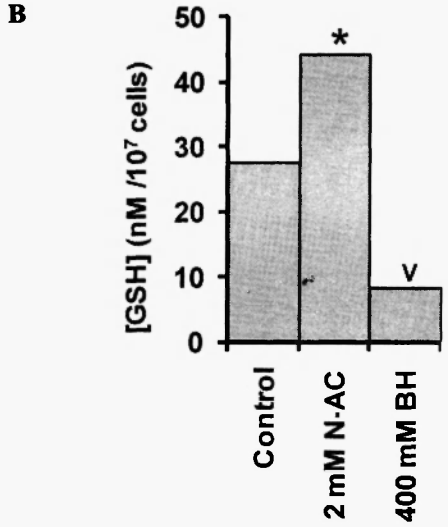

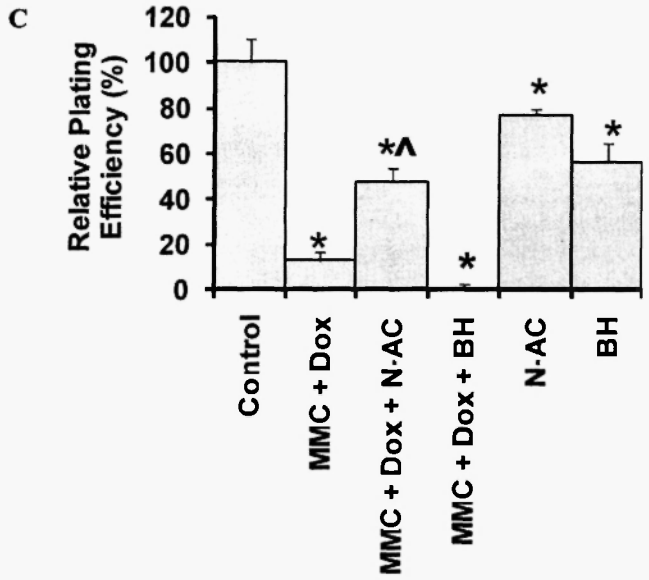

Fig. 4: Modulating cellular metabolic systems alters the efficacy of the co-administration of mitomycin C (MMC) and doxorubicin (DOX). **A.** Cellular evidence for a significant role of cytochrome P450 reductase and NAD(P)H quinone oxidoreductase 1 (NQO1) in the toxic action of 1.0 mM MMC and 0.5 mM DOX in EMT6 cells. Cells were pre-treated with 100 mM dicumarol (DIC) or 100 mM 1-aminobenzotriazole (ABT) for 1 hour. * Statistically significant increase relative to MMC and DOX alone ($p < 0.05$). **B.** The effect of the modulation of glutathione levels with *N*-acetylcysteine (N-AC) and 1-bromoheptane (BH) on EMT6 cells. The incubation of EMT6 cells with 2 mM N-AC or 400 μM BH for 2 hours resulted in increased and decreased levels of intracellular glutathione, respectively. **C.** The plating efficiency of EMT6 cells was measured in the presence and absence of the combination of 1.0 μM MMC and 0.5 μM DOX, with and without the modulation of glutathione, as described above. Data represent the mean + standard deviation of three independent trials. * Statistically significant decrease relative to control ($p < 0.05$); ^ statistically significant increase relative to MMC+DOX treatment ($p < 0.05$); ' statistically significant decrease relative to MMC+DOX treatment ($p < 0.05$).

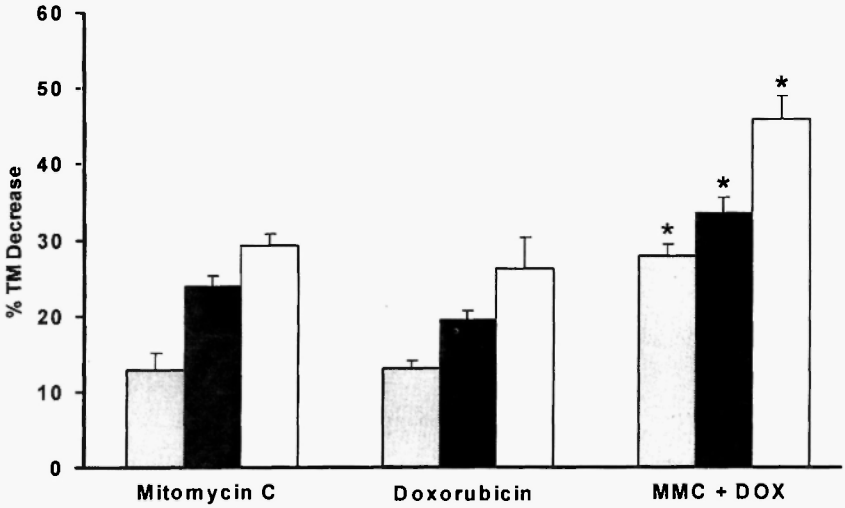

Fig. 5: The effect of mitomycin C (MMC) and doxorubicin (DOX) alone or in combination on the extent of DNA cross-linking from EMT6 cells as determined by a modified comet assay. Bars represent the % decrease in tail moment (TM) relative to untreated control. EMT6 cells were incubated for 1 hour with drug treatments: MMC (grey = 4 μM, black = 8 μM, white = 12 μM); DOX (grey = 2 μM, black = 4 μM, white = 6 μM); and a combination of both MMC and DOX (grey = 4.2 μM, black = 8.4 μM, white = 12.6 μM). Data represent the mean ± standard deviation of three independent trials. * Statistically significant decrease in tail moment relative to single treatments ($p < 0.001$).

DNA double-strand breaks

Previous reports of the ability of DOX to poison topoisomerase IIα and induce double-strand breaks necessitated investigation of this endpoint in the elucidation of the mechanism of drug interaction. At low doses (MMC: 4 μM, DOX: 2 μM) neither DOX nor MMC, alone or in combination, produced any significantly detectable amounts of DNA double-strand breaks above the untreated control (Fig. 6). At 8 μM MMC, DNA double-strand breaks were detected above the untreated control, and even more significantly when combined with 4 μM DOX. Even at this mid-dose level, DOX on its own was not able

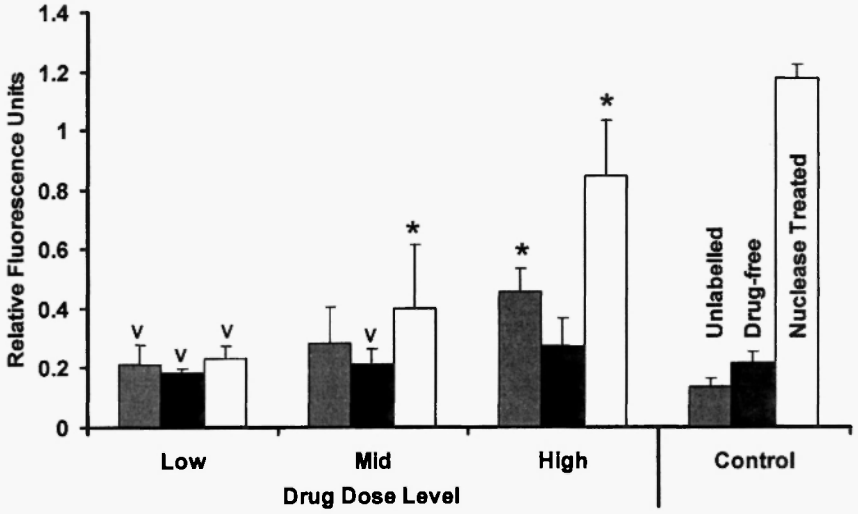

Fig. 6: DNA double-strand breaks in EMT6 cells as determined by the TUNEL assay. Bars represent the extent of double-strand break induction as a result of the metabolism of TACS-Sapphire™ by double-strand break-ligated horseradish peroxidase. EMT6 cells were incubated for 1 hour with low, mid, and high dose treatments of mitomycin C (MMC) alone (grey), doxorubicin (DOX) alone (black), or MMC and DOX in combination (white). Data represent the mean ± standard deviation of three independent trials. * Statistically significant increase in double-strand break induction relative to other drug treatments at the dose level ($p < 0.01$). ^{V} No significant difference relative to drug-free control ($p > 0.05$).

to produce a significant increase of double-strand breaks above the control. When EMT6 cells were exposed to 12 μM MMC and 6 μM DOX, both drugs produced significant levels of DNA double-strand breaks above the control. In addition, the combination treatment resulted in 112% increase in double-strand breaks relative to MMC on its own.

To account for the observed synergistic suppression of EMT6 clonogenicity upon exposure of the cells to both MMC and DOX, the specific toxic endpoint would be expected to have an effect, after treatment with the combination of agents, that is greater than the sum of the effect of each agent given alone. DNA double-strand breaks show this greater than additive effect when EMT6 cells were exposed

to both MMC and DOX ($p < 0.05$). This provides evidence that the institution of DNA double-strand breaks by the chemotherapeutic cocktail in question may be responsible for the observed synergistic effect of this combination.

DISCUSSION

Effects of drug dose

The present study has shown that the co-administration of MMC and DOX to EMT6 cells *in vitro* results in a synergistic enhancement of cell killing relative to administration of either of these drugs alone (Fig. 1B). However, the synergy appears to depend on whether the drug dose is higher or lower than the DOX dose causing less than 4% of tumor cell death when given alone. A lower combined efficacy of DOX and MMC (Fig. 1A) resulted from a DOX dose less than this threshold, while at this threshold, the combined effect was additive at best, progressing to antagonism at lower fractional efficacy. This result suggests that, in order to maintain clinical efficacy of this combination chemotherapy, doses yielding cell kill fractions beyond 5% are required. This observation may be explained by acquired drug resistance. At low doses of DOX, breast cancer cells acquire resistance to subsequent DOX exposure at clinically effective levels, as well as a cross-resistance to other drugs, such as MMC /43/.

Our study showed that the metabolism of MMC in subcellular fractions did not result in significant ROS production, differing from previous reports, and most likely due to drug dose differences. Briggs and Pristos /24/ reported that the ROS produced from MMC, in particular, in the microsomes and mitochondria, but not in the cytosol, were involved in the consumption of molecular oxygen. However, in these studies the concentration of MMC used was 300 μM, much more than the therapeutic dosing regimen would allow. In the clinic, the average dose of MMC and DOX applied, when used in *i.v.* combination therapy, is 10 mg/m^2 and 40 mg/m^2, respectively /44,45/, and the blood levels of DOX and MMC seen in the clinic are 6.0 μM /46/ and 10.4 μM /47/. In this work, 10-40 μM drug concentrations were studied. Although these concentrations are above the levels potentially reached in tumor cells, they are closer to the *in vivo* situation with *i.v.* drug administration than previous studies, and thus

may be more relevant to clinical conditions.

Role of GSH in the synergy

The specific role of GSH in the synergy of DOX and MMC could be explained by previously published findings. Lewandowicz *et al.* /44/ found that decreasing GSH can make resistant cells sensitive to DOX, even after exposure to previous failed rounds of DOX chemotherapy. This is probably because the acquired resistance of breast tumor cells to MMC and DOX depends on the overexpression of ATP-binding cassette efflux pumps /48,49/. These GSH-S-conjugate pumps require the conjugation of the drug to GSH /50/. Both DOX /51/ and MMC /52,53/ are capable of forming GSH-S adducts, and the intracellular levels of DOX have been shown to be highly dependent on the levels of intracellular GSH and the activity of the GSH-S conjugate efflux pump /51/. However, the drug efflux data obtained (Fig. 2) preclude any significant modulation of DOX efflux by MMC such that a pump-mediated mechanism of interaction cannot account for the synergy of the concurrent administration of these two drugs.

GSH plays an important role in the metabolism of MMC through the efficient formation of GSH-formaldehyde conjugates that act to non-enzymatically enhance the rate of bifunctional activation of MMC to form leucoaziridinomitosene, the metabolite formed with the loss of the MMC C_{11}-methoxy group /52,53/. This is associated with the formation of a ternary DNA adduct involving a MMC-GSH conjugate, as well as enhanced interstrand cross-linking over monoadduct formation in cell-free systems. The importance of GSH in modulating the toxic effects of DOX in human MCF-7 breast cancer cell lines has also been previously demonstrated with a different GSH-depleting system /54/. Using a combination of DOX and sodium butyrate, known to deplete GSH, combination index analyses demonstrated that when sodium butyrate and DOX were given concurrently or with a 24 h DOX pre-treatment, there was a significantly greater synergistic effect on decreasing clonogenic potential than if sodium butyrate was given 24 hours prior to DOX. Therefore, two different combinations of drugs with DOX that resulted in decreased GSH levels produce similar synergistic effects in two breast cancer cell lines from two different species, enhancing the importance of the proposed synergy between MMC and DOX.

Genotoxicity and the synergy of MMC and DOX

DOX has been shown to covalently link TIIα to DNA, forming a drug-protein-DNA ternary complex /41/. Consequently, the normally transient DNA double-strand break induced by TIIα becomes permanent and, upon collision with DNA polymerase, results in cytolethal protein-bound DNA double-strand breaks. DNA double-strand breaks were detected in EMT6 cells treated with MMC and DOX (Fig. 6), and the observed supra-additivity of DSBs upon combination treatment provides a toxic endpoint that can explain the observed synergy. DSBs have the potential to be incurred at increased frequency when MMC and DOX are used in combination due to the increased number of DNA adducts formed, and the increased activation of DNA repair machinery that occurs with DNA-drug binding events /55/. Experimental evidence obtained from ovarian cancer cell lines in which the absence of mismatch repair proteins resulted in resistance to DOX /56/ further strengthens the mechanism of interaction proposed here. Although in solo therapy, the toxicity of MMC correlates well with the extent of DNA interstrand cross-linking /21/, with poisoned TIIα stabilizing DNA DSBs, the monofunctional adducts of MMC could become more cytotoxic. It has been shown that MMC induces DNA repair within a few hours of the exposure of cells to the drug, and repair capacity greatly modifies the efficacy of MMC action /57/. The enhancement in toxicity of the chemotherapeutic cocktail can be explained by the additive increase in DNA crosslinking and drug-DNA adducts formed from MMC when combined with the cytolethal effects of DOX on TIIα functioning.

Proposed mechanism of interaction

Based on the findings from this study and in the literature, we propose a model for the mechanism of synergy between DOX and MMC as follows (Fig. 7). Formaldehyde is evolved from MMC during bioreductive metabolism. This can act to bind GSH, preventing the formation of GSH-S conjugates of DOX, resulting in its increased free intracellular concentration. DOX can then proceed to the nucleus to form the TIIα-DOX-DNA ternary complex, effectively stalling the enzyme on unwound DNA in the midst of strand scission. Alternatively, DOX can combine with the MMC-derived formaldehyde to form the genotoxin doxoform that can cross-link DNA. The bio-

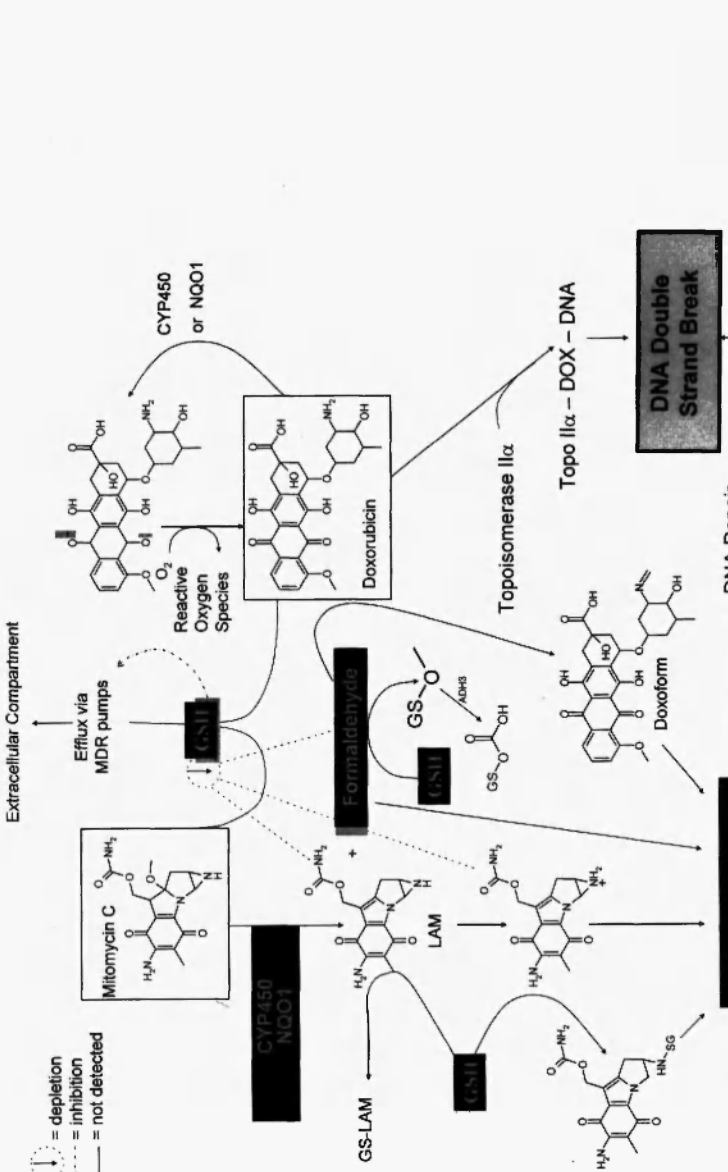

Fig. 7: Proposed mechanism of interaction between mitomycin C and doxorubicin (DOX). Glutathione (GSH) depletion by mitomycin C and its metabolites, including formaldehyde, act to prevent efflux of doxorubicin, allowing extensive poisoning of topoisomerase IIα. Mitomycin C, doxoform, and formaldehyde-protein adducts all bind DNA, activating DNA repair, and promoting collision of repair enzymes with stalled topoisomerase IIα, leading to lethal double-strand breaks in DNA.

activated MMC can also cross-link DNA, or form monoadducts or a GSH-DNA-MMC ternary complex. As a result, DNA repair machinery is activated to a greater extent when these drugs are given in combination than when they are given alone due to the significant increase in DNA adducts, providing ample opportunity for collision of DNA repair proteins with the stalled TIIα, leading to DNA double-strand breaks.

Importance of the timing of drug exposure

Previous work by Cheung *et al.* /7/ has shown that in EMT6 cells, synergy is greatest when MMC and DOX are given concurrently or when DOX is given before MMC, but not when MMC is given as a pretreatment to DOX. This result can be reconciled by the model proposed above. Pretreatment of EMT6 cells with MMC can lead to GSH depletion, as well as metabolism of MMC. It has been demonstrated that EMT6 cells can recover from GSH depletion within 20 to 60 minutes, recovering to basal thiol levels /58/. Therefore the GSH depletion to ensure the high intracellular concentration of active DOX afforded by MMC will be lost with preincubations of MMC that end more than 60 minutes before DOX exposure. As previously mentioned, MMC-induced DNA lesions can also be repaired within 4 hours of exposure to the drug. Any exposure to DOX beyond 4 hours to that of MMC may not culminate in the collision of stalled TIIα with MMC-DNA adducts. Additionally, the cellular kinetics of DOX uptake and efflux has been shown to result in a disproportionate equilibrium concentration of the drug, with intracellular concentrations being as much as 80-fold that of extracellular concentrations at low doses of DOX /59/. It is possible, then, that in culture, DOX will be maintained at toxic levels inside the cell while MMC depletes GSH levels, even if DOX is applied before MMC. Thus, the current model may be fitted to the observed dose interval-dependence of MMC and DOX using the known kinetics of drug accumulation in the cell and GSH regeneration.

CONCLUSION

This study has shown for the first time that the metabolism of MMC results in the production of formaldehyde, in addition to other

previously reported species. Specifically, it appears that NQO1 is the enzyme responsible for the majority of formaldehyde evolution from MMC, adding further weight to the importance of the two-electron reductive activation of this drug to its final toxic form. We have also shown that the supra-additive efficacy of the combination of DOX and MMC in breast cancer cells is in fact a true synergy. This synergy is ultimately mediated through the combination of MMC-induced initiation of DNA repair events with the DOX-mediated poisoning of TIIα, culminating in a synergistic amount of DNA double-strand breaks. This synergy was shown to be modulated by both glutathione levels and NQO1 activity; however, the exact nature of these effects is yet to be determined. The true synergy that exists between MMC and DOX may translate to lower clinical doses of these agents while maintaining high clinical efficacy for the treatment of breast cancer. Future work will focus on the rational design of this chemotherapeutic cocktail into an effective formulation of anti-cancer regimen relevant to the treatment of breast cancer.

ACKNOWLEDGEMENTS

This study was partly supported by CIHR to Drs. Wu and Rauth. Ontario Graduate Scholarship of Science and Technology and Ben Cohen Fund to A. Shuhendler are greatly acknowledged. The authors thank Dr. Peter G. Wells for the generous use of his cell incubator and cell culture facilities for the duration of the culture work required by this project; Dr. T Watts for the use of her gamma cell irradiator; Dr. J Uetrecht for the use of his UV/Vis and fluorescent microplate spectrometers; Dr. Robert G. Bristow for his valuable comments and expertise in clinical oncology; and Mr. A. Nagy for his technical assistance.

REFERENCES

1. Waterhouse DN, Gelmon KA, Klasa R, et al. Development and assessment of conventional and targeted drug combinations for use in the treatment of aggressive breast cancers. Curr Cancer Drug Targets 2006; 6: 455-489.
2. Tannock IF, Goldenberg GJ. Drug Resistance and Experimental Chemotherapy. Toronto: McGraw-Hill, 1998.

3. Rajagopal A, Simon SM. Subcellular localization and activity of multidrug resistance proteins. Mol Biol Cell 2003; 14: 3389-3399.
4. Tatebe S, Sinicrope F, Tien Kuo M. Induction of multidrug resistance proteins MRP1 and MRP3 and g-glutamylcysteine synthetase gene expression by non-steroidal anti-inflammatory drugs in human colon cancer cells. Biochem Biophys Res Commun 2002; 290: 1427-1433.
5. Andersson M, Daugaard S, von der Maase H, Mouridsen HT. Doxorubicin versus mitomycin versus doxorubicin plus mitomycin in advanced breast cancer: a randomized study. Cancer Treat Rep 1986; 70: 1181-1186.
6. Hortobagyi GN. Mitomycin: its evolving role in the treatment of breast cancer. Oncology 1993; 50: 1-8.
7. Cheung RY, Rauth AM, Ronaldson PT, Bendayan R, Wu XY. In vitro toxicity to breast cancer cells of microsphere-delivered mitomycin C and its combination with doxorubicin. Eur J Pharmaceut Biopharmaceut 2006; 62: 321-331.
8. Cheung RY, Rauth AM, Wu XY. In vivo efficacy and toxicity of intratumorally delivered mitomycin C and its combination with doxorubicin using microsphere formulations. Anti-Cancer Drugs 2005; 16: 1-11.
9. Cummings J, Spanswick VJ, Tomasz M, Smyth JF. Enzymology of mitomycin C metabolic activation in tumor tissue: implications for enzyme-directed bioreductive drug development. Biochem Pharmacol 1998; 56: 405-414.
10. Marshall RS, Paterson MC, Rauth AM. Deficient activation by a human cell strain leads to mitomycin resistance under aerobic but not hypoxic conditions. Br J Cancer 1989; 59: 341-346.
11. Cummings J, Willmott N, Hoey BM, Marley ES, Smyth JF. The consequences of doxorubicin quinone reduction in vivo in tumor tissue. Biochem Pharmacol 1992; 44: 2165-2174.
12. Gewirtz DA. A critical evaluation of the mechanisms of action proposed for the antitumor effects of the anthracycline antibiotics adriamycin and daunorubicin. Biochem Pharmacol 1999; 57: 727-774.
13. Garattini E, Donelli MG, Catalani P, Pantarotto C. Intact rat liver nuclei catalyze adriamycin irreversible interactions with DNA and nuclear proteins. Toxicol Lett 1983; 17: 343-348.
14. Cutts SM, Swift LP, Rephaeli A, Nudelman A, Phillips DR. Sequence specificity of adriamycin-DNA adducts in human tumor cells. Mol Cancer Ther 2003; 2: 661-670.
15. Kato S, Burke PJ, Henick DJ, Taatjes DJ, Bierbaum VM, Koch TH. Mass spectrometric measurement of formaldehyde generated in breast cancer cells upon treatment with anthracycline antitumor drugs. Chem Res Toxicol 2000; 13: 509-516.
16. Cutts SM, Rephaeli A, Nudelman A, Hmelnitsky I, Phillips DR. Molecular basis for the synergistic interaction of adriamycin with the formaldehyde-releasing prodrug pivaloyloxymethyl butyrate (AN-9). Cancer Res 2001; 61: 8194-8202.
17. Mitchell DY, Petersen DR. The oxidation of α,β-unsaturated aldehydic products of lipid peroxidation by rat liver aldehyde dehydrogenases. Toxicol Appl Pharmacol 1987; 87: 403-410.

18. Horning EC, Horning MG. Methone derivatives of aldehydes. J Org Chem 1961; 11: 95-99.
19. Bielski BHJ, Shiue GG, Bajuk S. Reduction of nitro blue tetrazolium by CO_2- and O_2-radicals. J Phys Chem 1980; 84: 830-833.
20. Reed DJ, Babson JR, Beatty PW, Brodie AE, Ellis WW, Potter DW. High-performance liquid chromatography analysis of nanomole levels of glutathione, glutathione disulfide, and related thiols and disulfides. Anal Biochem 1980; 106: 55-62.
21. Merk O, Speit G. Detection of crosslinks with the comet assay in relationship to genotoxicity and cytotoxicity. Environ Mol Mutagen 1999; 33: 167-172.
22. Riganti C, Miraglia E, Viarisio D, et al. Nitric oxide reverts the resistance to doxorubicin in human colon cancer cells by inhibiting the drug efflux. Cancer Res 2005; 65: 516-525.
23. Wielinga PR, Westerhoff HV, Lankelma J. The relative importance of passive and P-glycoprotein mediated anthracycline efflux from multidrug-resistant cells. Eur J Biochem 2000; 267: 649-657.
24. Bristow RG, Hill RP. Molecular and Cellular Basis of Radiotherapy. Toronto: McGraw-Hill, 1998.
25. Chou TC, Talalay P. Quantitative analysis of dose-effect relationships: the combined effects of multiple drugs or enzyme inhibitors. Adv Enzyme Regul 1984; 22: 27-55.
26. Chou TC. Theoretical basis, experimental design, and computerized simulation of synergism and antagonism in drug combination studies. Pharmacol Rev 2006; 58: 621-681.
27. Arceci RJ. Can multidrug resistance mechanisms be modified? Br J Hematol 2000; 110: 285-291.
28. Briggs LA, Pristos CA. Relative contributions of mouse liver subcellular fractions to the bioactivation of mitomycin C at various pH levels. Biochem Pharmacol 1999; 58: 1609-1614.
29. Hoey BM, Butler J, Swallow AJ. Reductive activation of mitomycin C. Biochemistry 1998; 27: 2608-2614.
30. Rauth AM, Melo T, Misra V. Bioreductive therapies: an overview of drugs and their mechanisms of action. Int J Radiat Oncol Biol Phys 1998; 42: 755-762.
31. Benchekroun MN, Sinha BK, Robert J. Doxorubicin-induced oxygen free radical formation in sensitive and doxorubicin-resistant variants of rat glioblastoma cell lines. FEBS Lett 1993; 322: 295-298.
32. Sawicki E, Carnes RA. Spectrofluorometric determination of aldehydes with dimedone and other reagents. Mikrochimica Acta [Wien] 1968; 1: 148-159.
33. Teng S, Beard K, Pourahmad J, et al. The formaldehyde metabolic detoxification enzyme systems and molecular cytotoxic mechanism in isolated rat hepatocytes. Chem Biol Interact 2001; 130-132: 285-296.
34. Saito Y, Nishio K, Yoshida Y, Niki E. Cytotoxic effect of formaldehyde with free radicals via increment of cellular reactive oxygen species. Toxicology 2005; 210: 235-245.

35. Ernster L, Ljunggren M, Davidson L. Purification and some properties of a highly dicumarol-sensitive liver diaphorase. Biochem Biophys Res Commun 1960; 2: 88-92.
36. Ayene IS, Stamato TD, Mouldin SK, et al. Mutation in glucose-6-phosphate dehydrogenase gene leads to inactivation of Ku DNA binding domain during oxidative stress. J Biol Chem 2002; 277: 9929-9935.
37. Salerno M, Garnier-Suillerot A. Kinetics of glutathione and daunorubicin efflux from multidrug resistance protein overexpressing small-cell lung cancer cells. Eur J Pharmacol 2001; 421: 1-9.
38. Horan AD, Koch CJ. The K_m for radiosensitization of human tumor cells by oxygen is much greater than 3 mmHg and is further increased by elevated levels of cysteine. Radiat Res 2001; 156: 388-398.
39. Cera C, Egbertson M, Teng SP, Crothers DM, Danishefsky TJ. DNA cross-linking by intermediates in the mitomycin C activation cascade. Biochemistry 1989; 28: 5665-5669.
40. Prakash AS, Beall H, Ross D, Gibson NW. Sequence-selective alkylation and cross-linking induced by mitomycin C upon activation by DT-diaphorase. Biochemistry 1993; 32: 5518-5528.
41. Moro S, Beretta GL, Ben DD, Nitiss J, Palumbo M, Capranico G. Interaction model for anthracycline activity against DNA topoisomerase II. Biochemistry 2004; 43: 7501-7513.
42. Palom Y, Belcourt MF, Tang LQ, et al. Bioreductive metabolism of mitomycin C in EMT6 mouse mammary tumor cells: cytotoxic and non-cytotoxic pathways, leading to different types of DNA adducts. The effect of dicumarol. Biochem Pharmacol 2001; 61: 1517-1529.
43. Kabanov AV, Batrakova EV, Alakhov VY. Pluronic block copolymers for overcoming drug resistance in cancer. Adv Drug Deliv Rev 2002; 54: 759-779.
44. Agency BC. DrugIndex (Professional): Mitomcyin C. http://www.bccancer.bc.ca/HPI/DrugDatabase/DrugIndexPro/Mitomycin.htm. January 12, 2006.
45. Agency BC. DrugIndex (Professional): Doxorubicin. http://www.bccancer.bc.ca/HPI/DrugDatabase/DrugIndexPro/Doxorubicin.htm. January 12, 2006.
46. Sato Y, Ohtsuka K, Ono K. Concentration of mitomycin C in portal blood and peripheral blood after intravenous, interperitoneal or intrapelvic administration. Gan To Kagaku Ryosho 1993; 20: 131-136.
47. Ackland SP, Ratain MJ, Vogelzang NJ, Choi KE, Ruane M, Sinkule JA. Pharmacokinetics and pharmacodynamics of long-term continuous-infusion doxorubicin. Clin Pharmacol Ther 1989; 45: 340-347.
48. Kanzaki A, Toi M, Nakayama K, et al. Expression of multidrug resistance-related transporters in human breast carcinoma. Jpn J Cancer Res 2001; 92: 452-458.
49. Linn SC, Pinedo HM, Van Arke-Otte J, et al. Expression of drug resistance proteins in breast cancer, in relation to chemotherapy. Int J Cancer 1997; 71: 787-795.

50. De Vries EG, Muller M, Meijer C, Jansen PL, Mulder NH. Role of the glutathione S-conjugate pump in cisplatin resistance. J Natl Cancer Inst 1995; 87: 537-538.
51. Sadzuka Y, Sugiyama T, Suzuki T, Sonobe T. Enhancement of the activity of doxorubicin by the inhibition of glutamate transporter. Toxicol Lett 2001; 123: 159-167.
52. Sharma M, He QY, Tomasz M. Effects of glutathione on alkylation and cross-linking of DNA by mitomycin C. Isolation of a ternary glutathione-mitomycin C-DNA adduct. Chem Res Toxicol 1994; 7: 401-407.
53. Sharma M, Tomasz M. Conjugation of glutathione and other thiols with bio-reductively activated mitomycin C. Effect of thiols on the reductive activation rate. Chem Res Toxicol 1994; 7: 390-400.
54. Louis M, Rosato RR, Battaglia E, et al. Modulation of sensitivity to doxo-rubicin by histone deacetylase inhibitor sodium butyrate in breast cancer cells. Int J Oncol 2005; 26: 1569-1574.
55. Bergman AM, Giaccone G, van Moorsel CJ, et al. Cross-resistance in the 2′,2′-difluorodeoxycytidine (gemcitabine)-resistant human ovarian cancer cell line AG6000 to standard and investigational drugs. Eur J Cancer 2000; 36: 1974-1983.
56. Drummond JT, Anthoney A, Brown R, Modrich P. Cisplatin and adriamycin resistance are associated with MutLa and mismatch repair deficiency in an ovarian tumor cell line. J Biol Chem 1996; 271: 19645-19648.
57. Kim SY, Rockwell S. Cytotoxic potential of monoalkylation products between mitomycins and DNA: studies of decarbamoyl mitomycin C in wild-type and repair-deficient cell lines. Oncol Res 1955; 7: 39-47.
58. Muller MR, Wright KA, Twentyman PR. Differential properties of cisplatin and tetraplatin with respect to cytotoxicity and perturbation of cellular gluta-thione levels. Cancer Chemother Pharmacol 1991; 28: 273-276.
59. Bates DA, Fung H, MacKillop WJ. Adriamycin uptake, intracellular binding and cytotoxicity in Chinese Hamster ovary cells. Cancer Lett 1985; 28: 213-221.